Continuous output feedback sliding mode control for underactuated flexible-joint robot

Huiming Wang[a,*], Zhize Zhang[a], Xianlun Tang[a], Zhenhua Zhao[b], Yunda Yan[c]

[a]*Chongqing Key Laboratory of Complex Systems and Bionic Control, Chongqing University of Posts and Telecommunications, Chongqing, China*
[b]*College of Automation Engineering, Nanjing University of Aeronautics and Astronautics, Nanjing, China*
[c]*Department of Aeronautical and Automotive Engineering, Loughborough University, Loughborough LE11 3TU, U.K.*

Abstract

The tracking control based on output feedback for a category of flexible-joint robot (FJR) systems is investigated in this brief. Control performance of the systems is inevitably bearing the brunt of various unknown time-varying disturbances, which can be categorized to be matched and mismatched and generally cover internal parameter uncertainties, couplings, unmodelled dynamics, and external load or changing operating environments. To cope with these disturbances, the mismatched disturbances are first transferred to the matched ones by a flatness method, which eliminates the computational cost of estimating mismatched disturbances. Then, a generalized proportional integral observer (GPIO) is constructed to estimate the unavailable states and disturbances. By integrating the estimated disturbance and states provided by the GPIO, a novel dynamic sliding surface is constructed. Finally, a continuous sliding mode control (CSMC)-based output feedback control framework is further designed. The presented control strategy only requires link position information and is continuous, which can effectively reduce the chattering driven by the high-frequency switching item in the traditional SMC method. Asymptotic convergence of output tracking error is guaranteed by theoretical analysis under some mild conditions. Comparative tests on a two-link FJR verify the claimed control performance.

Keywords: Continuous sliding mode control (CSMC), mismatched disturbance, generalized proportional integral observer (GPIO), flexible-joint robot (FJR).

1. Introduction

In the past several decades, flexible-joint robot (FJR) has been abundantly employed in human-robot interactions since it is designed to provide compliant behavior which guarantees human safety during human-robot interaction [1, 2]. Nevertheless, a flexible-joint robot (FJR) is a high-order and underactuated nonlinear system [3–5], which means that its order is twice that of the rigid one, and its actuator is fewer than the degrees of freedom to be controlled [6]. Meanwhile, an FJR system is often perturbed by all kinds of uncertainties and disturbances from the link side and actuator side, especially changing operating environments, couplings,

*Corresponding author at: Chongqing Key Laboratory of Complex Systems and Bionic Control, Chongqing University of Posts and Telecommunications, Chongqing, China
Email address: wanghm@cqupt.edu.cn (Huiming Wang)

and uncertainty of parameters [7]. The main motivation of this study is to develop a highly accurate tracking control scheme for the FJR system under the above intractable constraints.

With the booming growth of integrated circuits and computer technologies in recent years, it is feasible to design and employ advanced strategies to enhance the performance of mechatronic control systems, including the FJR, in different ways. For this purpose, a massive number of nonlinear control strategies have been utilized in flexible-joint (FJ) robotic systems, such as backstepping control [8], adaptive control [9, 10], neural network control [11], singular perturbation control [12, 13], passivity-based control [14]. A limitation of these control schemes is that speed sensors on the link and actuator are in demand. Nevertheless, it is known that speed measurements are generally eliminated in modern electromechanical devices due to the current requirements of reducing materials and maintenance costs [15]. Also, it is noted that the control performance of a system under most nonlinear feedback control methods will be degraded when severe disturbances are encountered. The reason is that these classic feedback control strategies are not to mitigate or fight off the undesirable impact of the disturbances on the control systems actively but to suppress them in a passive way [16–18]. These practical factors further increase the difficulty of controller design.

Among the existing nonlinear control strategies, sliding mode control (SMC) attracts numerous attention due to its inherent robustness against model errors, parameter uncertainties, and unknown external perturbations [19–23]. However, it is known that the chattering driven by switching items that exist in conventional SMC approaches is the main problem impeding its implementation. Correspondingly, a large variety of research works for chattering attenuation have been submitted to control the FJ robotic systems [24–26], such as high-order SMC method [27], boundary layer-based SMC approach [25], and observer-based SMC strategy [28]. Although the SMC scheme based on boundary layer can suppress the chattering behavior by substituting the saturation function for the switching item, this treatment can only guarantee that SMC is effective outside the boundary layer surrounding the sliding hyperplane, thus increasing the steady-state tracking error. By dint of adjusting the switching gain to a small one, the observer-based SMC strategy can reduce the chattering phenomenon to some extent, but this kind of control law is discontinuous in nature. The high-order SMC method achieves the purpose of continuity by placing the switching function in higher derivatives of the control law.

Another key problem with conventional SMC is that it can mitigate matched perturbations but cannot suppress unmatched perturbations entering the system via diverse channels from the control inputs [29–31]. To overcome this problem, the authors in [32] presented an adaptive SMC approach to dispose of mismatched disturbances via the backstepping-like design. Based on the cascaded structure, the authors in [33] developed an SMC scheme for FJ robotic systems suffering from mismatched disturbances. A disturbance observer-based SMC approach was constructed for a category of underactuated robots subject to unmatched disturbances [34]. A novel SMC scheme combined with the iterative learning technique was employed in [35] to improve the ability to suppress mismatched disturbances. These mentioned methods can diminish the adverse impact of mismatched perturbations added to FJR systems, but there is still potential for improving the control performance because the control laws are discontinuous, the disturbances are handled without an active manner, or the computational burden is increased.

Besides, considering that the control performance of the FJ robotic systems always suffers from various disturbances, many disturbance observation techniques have been addressed. For example, extended state observer (ESO) [36] and disturbance observer [37, 38] were proposed to observe constant disturbances or slow-varying disturbances, respectively. The difference between these two kinds of observers is that ESO can estimate system states in addition to distur-

bances, and disturbance observer needs to use the nominal model of the FJR [39]. Generalized proportional integral observer (GPIO) [7, 40] and finite-time disturbance observer (FTDO) [41] were developed to reconstruct time-varying perturbations, respectively. The main advantage of FTDO is that the exact estimates can be obtained in a finite time. However, it should be pointed out that FTDO is discontinuous, and the utilization of power function terms in FTDO increases the computational burden [42]. Therefore, considering the observation accuracy and computation burden, GPIO is an optimal scheme for estimating unmeasured states and time-varying disturbances.

In this paper, a continuous SMC (CSMC) approach based on output feedback is developed for the output of FJR systems to track its reference trajectory accurately. Firstly, to decrease the design burden of the subsequent observer and controller, a simplified model is proposed by a flatness approach, which transfers all the mismatched uncertainties/disturbances to the matched ones. Next on, a GPIO is developed to estimate the unmeasured states and total time-varying disturbance in unison. By introducing the estimated variables of the GPIO into a dynamic sliding hyperplane, the proposed CSMC scheme based on output feedback is finally devised. The contributions of our work are described below.

1) From the practical point of view, only a few parameters of the system model (i.e., the nominal values of inertia matrix of link side, flexible coefficient matrix, and inertia matrix of actuator side), the order of the system, as well as position measurements are required for the design of the GPIO and proposed controller;
2) In terms of theoretical innovation, the presented continuous controller can effectively solve the chattering phenomenon existing in conventional SMC methodology, which may damage the actuator and stimulate undesirable dynamics of a system, in addition to handling unknown matched/unmatched time-varying uncertainties/perturbations simultaneously;
3) Under the presented control method, a detailed theoretical analysis of the closed-loop stability of the system is given;
4) In comparison with the traditional active disturbance rejection control (ADRC) technique, test results illustrate that the presented control approach possesses superior control performance concerning trajectory tracking precision and robustness.

The rest of this note is outlined next. The dynamic of a category of n-link FJR systems and problem formulation is presented in Section 2. Section 3 introduces the design procedure of the output feedback control framework, consisting of a GPIO, a dynamic sliding hyperplane, and a CSMC law, and analyzes the closed-loop stability. Section 4 gives the simulation results of the proposed scheme and the ADRC scheme. A brief conclusion is in Section 5.

Notations: Throughout this brief, $\mathbb{R}$, $\mathbb{R}^n$, and $\mathbb{R}^{n\times n}$ separately represent the real number, n-vector, and n-matrix spaces; L_∞ refers to the space of bound signals; $\|\cdot\|$ denotes Euclid norm; sign$(\cdot)$ is a standard signum function; $\boldsymbol{f}^{(i)} = \frac{d^i \boldsymbol{f}}{dt^i}$.

2. Model description and problem formulation

The dynamic equation of a class of n-link FJ robotic systems is first introduced, and then problem formulation based on a standard model is presented. Some widely held assumptions are also detailed.

2.1. Model description of FJR

Through the Euler-Lagrange equations, the mathematical equation of an n-link underactuated FJR system, consisting of the link- and motor-side dynamics, is depicted by [1]

$$\begin{cases} \boldsymbol{M}(\boldsymbol{q}_l)\ddot{\boldsymbol{q}}_l + \boldsymbol{C}(\boldsymbol{q}_l, \dot{\boldsymbol{q}}_l)\dot{\boldsymbol{q}}_l + \boldsymbol{G}(\boldsymbol{q}_l) = \boldsymbol{K}(\boldsymbol{q}_m - \boldsymbol{q}_l) + \boldsymbol{d}_1, \\ \quad \boldsymbol{J}\ddot{\boldsymbol{q}}_m + \boldsymbol{B}\dot{\boldsymbol{q}}_m + \boldsymbol{K}(\boldsymbol{q}_m - \boldsymbol{q}_l) = \boldsymbol{\tau} + \boldsymbol{d}_2, \end{cases} \tag{1}$$

where $\boldsymbol{q}_l$ and $\boldsymbol{q}_m$ refer to the link and motor positions, respectively; The Coriolis-centripetal matrix, inertia matrix, and gravity vector of the rigid link are separately denoted by $\boldsymbol{C}(\boldsymbol{q}_l, \dot{\boldsymbol{q}}_l) \in \mathbb{R}^{n\times n}$, $\boldsymbol{M}(\boldsymbol{q}_l) \in \mathbb{R}^{n\times n}$, and $\boldsymbol{G}(\boldsymbol{q}_l) \in \mathbb{R}^n$; $\boldsymbol{B} \in \mathbb{R}^{n\times n}$, $\boldsymbol{J} \in \mathbb{R}^{n\times n}$, and $\boldsymbol{K} \in \mathbb{R}^{n\times n}$ denote the natural damping terms, inertia matrix, and flexible coefficient matrix of the actuator side, respectively; $\boldsymbol{d}_1 \in \mathbb{R}^n$ and $\boldsymbol{d}_2 \in \mathbb{R}^n$ represent external disturbances separately added to the link and actuator; $\boldsymbol{\tau} \in \mathbb{R}^n$ is the control input or the motor torque. It is assumed that only $\boldsymbol{q}_l$ is measurable in this work.

Property 1 [12]: $\boldsymbol{M}(\boldsymbol{q}_l)$ is positive, symmetric, $\forall \boldsymbol{q}_l \in \mathbb{R}^n$, and $\boldsymbol{K}$ and $\boldsymbol{J}$ are positive, diagonal.

Assumption 1 [43]: The matrices $\boldsymbol{M}(\boldsymbol{q}_l)$, $\boldsymbol{K}$, and $\boldsymbol{J}$ subject to unknown time-varying disruptions and are expressed as $\boldsymbol{M}(\boldsymbol{q}_l) = \boldsymbol{M}_0(\boldsymbol{q}_l) + \Delta\boldsymbol{M}(\boldsymbol{q}_l)$, $\boldsymbol{J} = \boldsymbol{J}_0 + \Delta\boldsymbol{J}$, and $\boldsymbol{K} = \boldsymbol{K}_0 + \Delta\boldsymbol{K}$, respectively, where $\boldsymbol{M}_0(\boldsymbol{q}_l)$, $\boldsymbol{J}_0$ and $\boldsymbol{K}_0$ denote the nominal values; $\Delta\boldsymbol{M}(\boldsymbol{q}_l)$, $\Delta\boldsymbol{J}$ and $\Delta\boldsymbol{K}$ denote the unknown time-varying uncertainties.

Assumption 2 [7]: Suppose that $\boldsymbol{q}_r^{(i)}(i = 0, 1, \cdots .4)$ is of L_∞, where $\boldsymbol{q}_r = [q_{r1}, q_{r2}, \cdots, q_{rn}] \in \mathbb{R}^n$ represent a given reference trajectory.

2.2. Problem formulation

Defining $\boldsymbol{x}_1 = \boldsymbol{q}_l$, $\boldsymbol{x}_2 = \dot{\boldsymbol{q}}_l$, $\boldsymbol{x}_3 = \boldsymbol{q}_m$, and $\boldsymbol{x}_4 = \dot{\boldsymbol{q}}_m$, we rearrange dynamic model (1) as

$$\begin{cases} \dot{\boldsymbol{x}}_1 = \boldsymbol{x}_2, \\ \dot{\boldsymbol{x}}_2 = \boldsymbol{M}^{-1}(\boldsymbol{x}_1)(\boldsymbol{K}(\boldsymbol{x}_3 - \boldsymbol{x}_1) - \boldsymbol{C}(\boldsymbol{x}_1, \boldsymbol{x}_2)\boldsymbol{x}_2 \\ \qquad - \boldsymbol{G}(\boldsymbol{x}_1) + \boldsymbol{d}_1), \\ \dot{\boldsymbol{x}}_3 = \boldsymbol{x}_4, \\ \dot{\boldsymbol{x}}_4 = \boldsymbol{J}^{-1}(\boldsymbol{\tau} - \boldsymbol{B}\boldsymbol{x}_4 - \boldsymbol{K}(\boldsymbol{x}_3 - \boldsymbol{x}_1) + \boldsymbol{d}_2). \end{cases} \tag{2}$$

which is a differentially flat system [44], and $\boldsymbol{q}_l$ is the flat output which is redefined as $\boldsymbol{\Lambda}$. Hence, we can formulate all the variables containing state $\boldsymbol{x}_i$ and control input $\boldsymbol{\tau}$ by

$$\begin{aligned} \boldsymbol{x}_1 &= \boldsymbol{\Lambda}, \quad \boldsymbol{x}_2 = \dot{\boldsymbol{\Lambda}}, \\ \boldsymbol{x}_3 &= \boldsymbol{K}^{-1}\left(\boldsymbol{M}(\boldsymbol{\Lambda})\ddot{\boldsymbol{\Lambda}} + \boldsymbol{C}(\boldsymbol{\Lambda}, \dot{\boldsymbol{\Lambda}})\dot{\boldsymbol{\Lambda}}\right. \\ &\quad \left. + \boldsymbol{K}\boldsymbol{\Lambda} + \boldsymbol{G}(\boldsymbol{\Lambda}) - \boldsymbol{d}_1\right), \\ \boldsymbol{x}_4 &= \boldsymbol{K}^{-1}\left(\boldsymbol{M}(\boldsymbol{\Lambda})\boldsymbol{\Lambda}^{(3)} + \dot{\boldsymbol{M}}(\boldsymbol{\Lambda})\ddot{\boldsymbol{\Lambda}} + \boldsymbol{C}\left(\boldsymbol{\Lambda}, \dot{\boldsymbol{\Lambda}}\right)\ddot{\boldsymbol{\Lambda}}\right. \\ &\quad \left. + \dot{\boldsymbol{C}}\left(\boldsymbol{\Lambda}, \dot{\boldsymbol{\Lambda}}\right)\dot{\boldsymbol{\Lambda}} + \boldsymbol{\Lambda}\dot{\boldsymbol{\Lambda}} + \dot{\boldsymbol{G}}(\boldsymbol{\Lambda}) - \dot{\boldsymbol{d}}_1\right), \\ \boldsymbol{\tau} &= \frac{\boldsymbol{J}\boldsymbol{M}(\boldsymbol{\Lambda})}{\boldsymbol{K}}\boldsymbol{\Lambda}^{(4)} + \boldsymbol{\Gamma}\left(\boldsymbol{\Lambda}^{(3)}, \ddot{\boldsymbol{\Lambda}}, \dot{\boldsymbol{\Lambda}}, \boldsymbol{\Lambda}, \ddot{\boldsymbol{M}}(\boldsymbol{\Lambda}), \dot{\boldsymbol{M}}(\boldsymbol{\Lambda}),\right. \\ &\quad \boldsymbol{M}(\boldsymbol{\Lambda}), \ddot{\boldsymbol{C}}(\boldsymbol{\Lambda}, \dot{\boldsymbol{\Lambda}}), \dot{\boldsymbol{C}}(\boldsymbol{\Lambda}, \dot{\boldsymbol{\Lambda}}), \boldsymbol{C}(\boldsymbol{\Lambda}, \dot{\boldsymbol{\Lambda}}), \ddot{\boldsymbol{G}}(\boldsymbol{\Lambda}), \\ &\quad \left.\dot{\boldsymbol{G}}(\boldsymbol{\Lambda}), \boldsymbol{G}(\boldsymbol{\Lambda}), \boldsymbol{K}, \boldsymbol{J}, \boldsymbol{B}, \ddot{\boldsymbol{d}}_1, \dot{\boldsymbol{d}}_1, \boldsymbol{d}_1, \boldsymbol{d}_2\right), \end{aligned} \tag{3}$$

where $\boldsymbol{C}(\boldsymbol{\Lambda}, \dot{\boldsymbol{F}})$, $\boldsymbol{M}(\boldsymbol{\Lambda})$, $\boldsymbol{G}(\boldsymbol{\Lambda})$, $\boldsymbol{B}$, $\boldsymbol{\Lambda}$, $\boldsymbol{K}$, $\boldsymbol{J}$, $\boldsymbol{d}_1$, $\boldsymbol{d}_2$, and corresponding time derivatives are arguments of function $\boldsymbol{\Gamma}(\cdot)$, and a detailed expression for $\boldsymbol{\tau}$ is provided in Appendix for readability.

Recall **Assumption 1**, dynamic (3) is governed by the following simplified form

$$\boldsymbol{\Lambda}^{(4)} = \boldsymbol{\alpha}\boldsymbol{\tau} + \boldsymbol{\xi}(t), \tag{4}$$

where $\boldsymbol{\alpha} = \boldsymbol{K}_0/(\boldsymbol{M}_0(\boldsymbol{\Lambda})\boldsymbol{J}_0)$, $\boldsymbol{\xi}(t) = (\boldsymbol{K}/(\boldsymbol{M}(\boldsymbol{\Lambda})\boldsymbol{J}) - \boldsymbol{K}_0/(\boldsymbol{M}_0(\boldsymbol{\Lambda})\boldsymbol{J}_0))\boldsymbol{\tau} - (\boldsymbol{K}/(\boldsymbol{M}(\boldsymbol{\Lambda})\ \boldsymbol{J}))\boldsymbol{\Gamma}(\cdot)$ is deemed to be a lumped time-varying disturbance covering parameter variations, varying operating environment, and unmodelled dynamics.

Assumption 3: Disturbance $\boldsymbol{\xi}(t)$ in system (4) is bounded and m times differentiable, where $\lim_{t\to\infty} \|\boldsymbol{\xi}^{(m)}(t)\| = 0$.

Remark 1: Assumption 3 indicates that disturbance and its rate of change are invariably finite in the real world. It is a broad internal model solution held by the higher-order disturbance estimation technique [7, 45]. Besides, order m of $\boldsymbol{\xi}(t)$ should be selected based on the character of the disturbances. To express the diverse forms of disturbances, for example, constant, ramp, parabolic, and their combinations, we can set order $m = 1$, 2, and 3, respectively. Generally speaking, choosing a larger m value can obtain a higher observation accuracy, but this treatment will correspondingly bring the computational burden. Therefore, in practical application, a tradeoff between observation precision and computational costs should be considered.

The ultimate goal of this note is to develop a concise control scheme for the underactuated FJ robotic system (1) such that output trajectory $\boldsymbol{q}_l$ follows its reference trajectory $\boldsymbol{q}_r$ well in the existence of total disturbance $\boldsymbol{\xi}(t)$.

3. Main results

The robust output feedback control scheme divided into several steps is provided. First, an augmented state-space model is presented for the subsequent observer and controller design. Second, we construct a GPIO for estimating the unmeasurable states as well as the lumped disturbance. Third, with the estimates provided by the GPIO, a concise output feedback controller is designed by introducing a CSMC technique. Finally, a theoretical analysis of the closed-loop stability analysis is provided.

3.1. Controller design

Recalling **Assumption 3**, we can define the following set of auxiliary variables

$$\boldsymbol{\xi}_0 = \boldsymbol{\xi}(t),\ \boldsymbol{\xi}_1 = \dot{\boldsymbol{\xi}}(t),\ \cdots,\ \boldsymbol{\xi}_{m-1} = \boldsymbol{\xi}^{(m-1)}(t).$$

Based on system (4), we can obtain the augmented state-space system:

$$\begin{cases} \dot{\boldsymbol{\Lambda}}_i = \boldsymbol{\Lambda}_{i+1},\ i = 0, 1, 2 \\ \dot{\boldsymbol{\Lambda}}_3 = \boldsymbol{\xi}_0 + \boldsymbol{\alpha}\boldsymbol{\tau}, \\ \dot{\boldsymbol{\xi}}_j = \boldsymbol{\xi}_{j+1},\ j = 0, 1, \cdots, m-2, \\ \dot{\boldsymbol{\xi}}_{m-1} = \boldsymbol{\xi}^{(m)}(t), \end{cases} \tag{5}$$

where $\boldsymbol{\Lambda}_0 = \boldsymbol{\Lambda}$, $\boldsymbol{\Lambda}_1 = \dot{\boldsymbol{\Lambda}}$, $\boldsymbol{\Lambda}_2 = \ddot{\boldsymbol{\Lambda}}$, $\boldsymbol{\Lambda}_3 = \boldsymbol{\Lambda}^{(3)}$.

The GPIO presented by [7] is an effective way for estimating time-varying perturbation and unmeasured states in (5), where $\boldsymbol{\Lambda}_i$ and $\boldsymbol{\xi}_j$ are estimated by

$$\begin{cases} \dot{\hat{\boldsymbol{\Lambda}}}_i = \hat{\boldsymbol{\Lambda}}_{i+1} - \boldsymbol{L}_{m+3-i}(\hat{\boldsymbol{\Lambda}}_0 - \boldsymbol{\Lambda}_0), \\ \dot{\hat{\boldsymbol{\Lambda}}}_3 = \hat{\boldsymbol{\xi}}_0 + \boldsymbol{\alpha}\boldsymbol{\tau} - \boldsymbol{L}_m(\hat{\boldsymbol{\Lambda}}_0 - \boldsymbol{\Lambda}_0), \\ \dot{\hat{\boldsymbol{\xi}}}_j = \hat{\boldsymbol{\xi}}_{j+1} - \boldsymbol{L}_{m-1-j}(\hat{\boldsymbol{\Lambda}}_0 - \boldsymbol{\Lambda}_0), \\ \dot{\hat{\boldsymbol{\xi}}}_{m-1} = -\boldsymbol{L}_0(\hat{\boldsymbol{\Lambda}}_0 - \boldsymbol{\Lambda}_0), \end{cases} \tag{6}$$

where $\hat{\boldsymbol{\Lambda}}_0$, $\hat{\boldsymbol{\Lambda}}_1$, $\hat{\boldsymbol{\Lambda}}_2$, $\hat{\boldsymbol{\Lambda}}_3$ are the estimates of $\boldsymbol{\Lambda}_0$, $\boldsymbol{\Lambda}_1$, $\boldsymbol{\Lambda}_2$, $\boldsymbol{\Lambda}_3$, respectively; $\hat{\boldsymbol{\xi}}_0, \hat{\boldsymbol{\xi}}_1, \cdots, \hat{\boldsymbol{\xi}}_{m-1}$ are the estimates of $\boldsymbol{\xi}_0, \boldsymbol{\xi}_1, \cdots, \boldsymbol{\xi}_{m-1}$, respectively; $\boldsymbol{L}_i = \text{diag}(L_{i1}, L_{i2}, \cdots, L_{in})$, $L_{i1}, L_{i2}, \cdots, L_{in} > 0$, $(i = 0, 1, \cdots, m+3)$, are observer coefficients, which can be determined such that the polynomials

$$s^{m+4} + L_{(m+3)k}s^3 + L_{(m+2)k}s^2 + \cdots + L_{1k}s + L_{0k}, \ (k = 1, 2, \cdots, n)$$

are Hurwitz stable.

The observer estimation errors of (5) and (6) are denoted by

$$\begin{cases} \dot{\boldsymbol{E}}_{\Lambda_i} = \boldsymbol{E}_{\Lambda_{i+1}} - \boldsymbol{L}_{m+3-i}\boldsymbol{E}_{\Lambda_0}, \\ \dot{\boldsymbol{E}}_{\Lambda_3} = \boldsymbol{E}_{\xi_0} - \boldsymbol{L}_m\boldsymbol{E}_{\Lambda_0}, \\ \dot{\boldsymbol{E}}_{\xi_j} = \boldsymbol{E}_{\xi_{j+1}} - \boldsymbol{L}_{m-1-j}\boldsymbol{E}_{\Lambda_0}, \\ \dot{\boldsymbol{E}}_{\xi_{m-1}} = -\boldsymbol{\xi}^{(m)}(t) - \boldsymbol{L}_0\boldsymbol{E}_{\Lambda_0}, \end{cases} \tag{7}$$

where $\boldsymbol{E}_{\Lambda_i} = \hat{\boldsymbol{\Lambda}}_i - \boldsymbol{\Lambda}_i, (i = 0, 1, 2, 3)$, $\boldsymbol{E}_{\xi_j} = \hat{\boldsymbol{\xi}}_j - \boldsymbol{\xi}_j, (j = 0, 1, \cdots, m-1)$. Letting $\boldsymbol{E} = [\boldsymbol{E}_{\Lambda_0}^T, \cdots, \boldsymbol{E}_{\Lambda_3}^T, \boldsymbol{E}_{\xi_0}^T, \cdots, \boldsymbol{E}_{\xi_{m-1}}^T]^T$, we have

$$\dot{\boldsymbol{E}} = \boldsymbol{A}\boldsymbol{E} + \boldsymbol{B}\boldsymbol{\xi}^m(t), \tag{8}$$

where

$$\boldsymbol{A} = \begin{bmatrix} -\boldsymbol{L}_{m+3} & \boldsymbol{I} & \boldsymbol{0} & \cdots & \boldsymbol{0} \\ -\boldsymbol{L}_{m+2} & \boldsymbol{0} & \boldsymbol{I} & \cdots & \boldsymbol{0} \\ \vdots & \vdots & \vdots & \ddots & \vdots \\ -\boldsymbol{L}_1 & \boldsymbol{0} & \boldsymbol{0} & \boldsymbol{0} & \boldsymbol{I} \\ -\boldsymbol{L}_0 & \boldsymbol{0} & \boldsymbol{0} & \boldsymbol{0} & \boldsymbol{0} \end{bmatrix}, \boldsymbol{B} = \begin{bmatrix} \boldsymbol{0} \\ \boldsymbol{0} \\ \vdots \\ \boldsymbol{0} \\ -\boldsymbol{I} \end{bmatrix}.$$

Notice that $\boldsymbol{A}$ is Hurwitz. Then, there exists a positive symmetric matrix $\boldsymbol{P}$ such that the equation $\boldsymbol{A}^T\boldsymbol{P} + \boldsymbol{P}\boldsymbol{A} = -\boldsymbol{I}$ holds. We choose a quadratic Lyapunov function $V_e(\boldsymbol{E}) = \boldsymbol{E}^T\boldsymbol{P}\boldsymbol{E}$ that implies the property $V_e(\boldsymbol{E})/\lambda_{\max}(\boldsymbol{P}) \le \|\boldsymbol{E}\|^2 \le V_e(\boldsymbol{E})/\lambda_{\min}(\boldsymbol{P})$, where $\lambda_{\min}(\boldsymbol{P})$ and $\lambda_{\max}(\boldsymbol{P})$ respectively represent the minimum and maximum eigenvalues of matrix $\boldsymbol{P}$.

Taking the derivative of $V_e(\boldsymbol{E})$ gives

$$\begin{aligned} \dot{V}_e(\boldsymbol{E}) &\le -\|\boldsymbol{E}\|^2 + 2\lambda_{\max}(\boldsymbol{P})\|\boldsymbol{E}\| \, \|\boldsymbol{\xi}^{(m)}(t)\| \\ &\le -\|\boldsymbol{E}\|^2 + \lambda_{\max}(\boldsymbol{P})\|\boldsymbol{E}\|^2 + \lambda_{\max}(\boldsymbol{P})\|\boldsymbol{\xi}^{(m)}(t)\|^2 \\ &\le -(1 - \lambda_{\max}(\boldsymbol{P}))\|\boldsymbol{E}\|^2 + \lambda_{\max}(\boldsymbol{P})\|\boldsymbol{\xi}^{(m)}(t)\|^2 \\ &\le -(\frac{1}{\lambda_{\max}(\boldsymbol{P})} - 1)V(\boldsymbol{E}) + \lambda_{\max}(\boldsymbol{P})\|\boldsymbol{\xi}^{(m)}(t)\|^2. \end{aligned} \tag{9}$$

From formula (9), we obtain

$$V_e(\boldsymbol{E}) \le \frac{\lambda_{\max}^2(\boldsymbol{P})\|\boldsymbol{\xi}^{(m)}(t)\|^2}{1 - \lambda_{\max}(\boldsymbol{P})} + (V_e(\boldsymbol{E}(0)) - \frac{\lambda_{\max}^2(\boldsymbol{P})\|\boldsymbol{\xi}^{(m)}(t)\|^2}{1 - \lambda_{\max}(\boldsymbol{P})})e^{-[\frac{1}{\lambda_{\max}(\boldsymbol{P})} - 1]t}, \tag{10}$$

and the convergence region (denoted as $\mathcal{B}$) of error $\boldsymbol{E}$ can be further deduced by

$$\mathcal{B} = \left\{ \boldsymbol{E} \;\middle|\; \|\boldsymbol{E}\|^2 \le \frac{\lambda_{\max}^2(\boldsymbol{P})\|\boldsymbol{\xi}^{(m)}(t)\|^2}{\lambda_{\min}(\boldsymbol{P})(1 - \lambda_{\max}(\boldsymbol{P}))} \right\}, \tag{11}$$

which means $\boldsymbol{E}$ will converge to the bounded region $\mathcal{B}$ in an exponential manner. Since the disturbance $\boldsymbol{\xi}(t)$ in system (4) satisfies **Assumption 3**, it follows from formula (11) that the

states of GPIO (6) can track its real states in (5) asymptotically by configuring appropriate coefficient $\boldsymbol{L}_i$ [46], that is $\lim_{t\to\infty} \boldsymbol{E}_{\Lambda_i}(t) = \boldsymbol{0}$, $\lim_{t\to\infty} \boldsymbol{E}_{\xi_j}(t) = \boldsymbol{0}$.

With the estimations given by the GPIO, a novel dynamic sliding surface is constructed by

$$\boldsymbol{S} = [S_1, \cdots, S_n]^T = \boldsymbol{\Lambda}_r^{(4)} - (\boldsymbol{\alpha}\boldsymbol{\tau} + \hat{\boldsymbol{\xi}}_0) + \sum_{i=1}^{3} \boldsymbol{H}_i(\boldsymbol{\Lambda}_r^{(i)} - \hat{\boldsymbol{\Lambda}}_i) + \boldsymbol{H}_0(\boldsymbol{\Lambda}_r - \boldsymbol{\Lambda}_0), \tag{12}$$

where $\boldsymbol{\Lambda}_r = \boldsymbol{q}_r$ stands for a given reference trajectory, $\boldsymbol{H}_i = \mathrm{diag}(H_{i1}, H_{i2}, \cdots, H_{in})$, H_{i1}, H_{i2}, $\cdots$, $H_{in} > 0$, $(i = 0, 1, 2, 3)$ are the coefficients, which can be selected such that the polynomials

$$s^4 + H_{3k}s^3 + H_{2k}s^2 + H_{1k}s + H_{0k}, \ (k = 1, 2, \cdots, n)$$

are Hurwitz stable.

Next on, a proposed output feedback control law is designed by integrating the CSMC technique [47] and disturbance observations (6), which is formulated by

$$\begin{cases} \boldsymbol{\tau} = \boldsymbol{\alpha}^{-1}(\boldsymbol{\tau}_{eq} + \boldsymbol{\tau}_v), \\ \boldsymbol{\tau}_{eq} = \boldsymbol{\Lambda}_r^{(4)} + \sum_{i=1}^{3} \boldsymbol{H}_i(\boldsymbol{\Lambda}_r^{(i)} - \hat{\boldsymbol{\Lambda}}_i) + \boldsymbol{H}_0(\boldsymbol{\Lambda}_r - \boldsymbol{\Lambda}_0) - \hat{\boldsymbol{\xi}}_0, \\ \dot{\boldsymbol{\tau}}_v = \boldsymbol{\lambda}\mathrm{sign}(\boldsymbol{S}), \end{cases} \tag{13}$$

with $\boldsymbol{\lambda} = \mathrm{diag}(\lambda_1, \lambda_2, \cdots, \lambda_n)$ the control gain.

The block diagram of the FJ robotic system under the presented control scheme is illustrated in Fig. 1, which mainly includes model transformation and controller design. Model transformation converts mismatched disturbances in formula (1) to a lumped matched disturbance as shown in formula (5). For controller design, observer (6) is first constructed based on formula (5), and then sliding mode surface (12) and CSMC law (13) are developed based on the observation results.

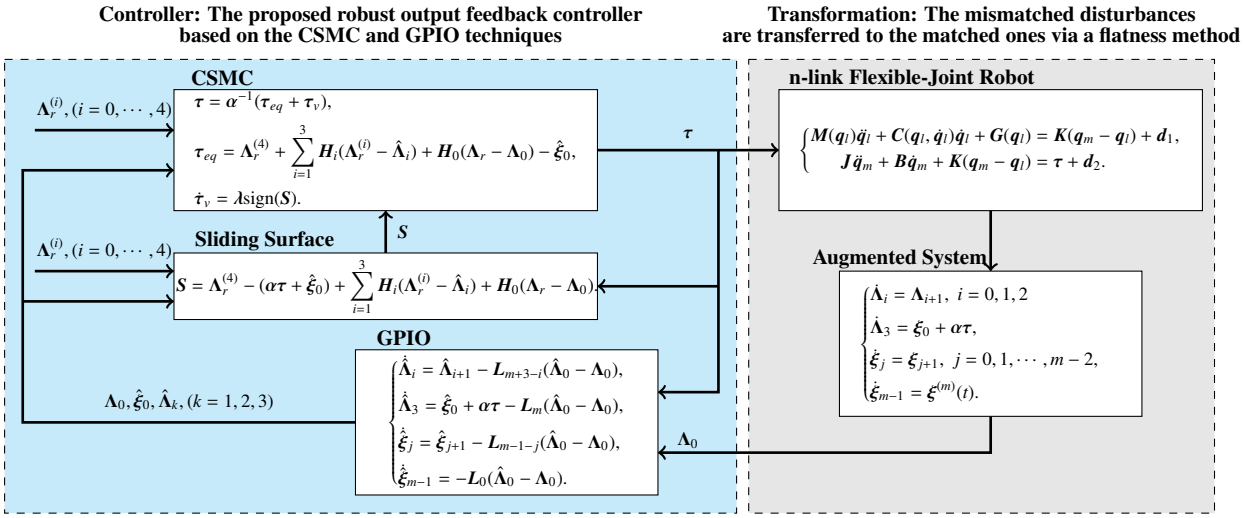

Figure 1: Block diagram of the presented output feedback control approach based on the CSMC, GPIO, and flatness techniques

3.2. Stability analysis

Lemma 1 [48]: Inequality $(|\gamma_1| + |\gamma_2| + \cdots + |\gamma_n|)^\alpha \leq |\gamma_1|^\alpha + |\gamma_2|^\alpha + \cdots + |\gamma_n|^\alpha$ holds for $\gamma_i (i = 1, 2, \cdots, n) \in \mathbb{R}$ and $0 < \alpha \leq 1$ a constant.

Lemma 2 [49]: Suppose that a system $\dot{x} = f(x, \upsilon(t))$ is input-to-state stable (ISS). If condition $\lim_{t\to\infty} \upsilon(t) = 0$ is satisfied, it yields $\lim_{t\to\infty} x(t) = 0$.

Theorem 1: For FJ robotic system (1), **Assumptions 1-3** are satisfied, and parameter uncertainties and time-varying disturbances are unknown. With the appropriate coefficients $\{\boldsymbol{L}_0, \boldsymbol{L}_1, \cdots, \boldsymbol{L}_{m+3}\}$ and $\{\boldsymbol{H}_0, \boldsymbol{H}_1, \boldsymbol{H}_2, \boldsymbol{H}_3\}$, the proposed control method including the observer (6), sliding mode surface (12), and control law (13) ensures that link position $\boldsymbol{q}_l$ of the system asymptotically converges to the reference trajectory $\boldsymbol{q}_r$ if the gain $\lambda_i > 0$.

Proof: Substituting (13) into (12), yields

$$\begin{aligned} \boldsymbol{S} &= \boldsymbol{\Lambda}_r^{(4)} - (\boldsymbol{\tau}_{eq} + \boldsymbol{\tau}_v + \hat{\boldsymbol{\xi}}_0) \\ &\quad + \sum_{i=1}^{3} \boldsymbol{H}_i(\boldsymbol{\Lambda}_r^{(i)} - \hat{\boldsymbol{\Lambda}}_i) + \boldsymbol{H}_0(\boldsymbol{\Lambda}_r - \boldsymbol{\Lambda}_0) \\ &= -\boldsymbol{\tau}_v, \end{aligned} \tag{14}$$

and then taking the derivative of $\boldsymbol{S}$, yields

$$\dot{\boldsymbol{S}} = -\boldsymbol{\lambda}\text{sign}(\boldsymbol{S}). \tag{15}$$

A Lyapunov function can be defined as

$$V(\boldsymbol{S}) = (1/2)\boldsymbol{S}^T\boldsymbol{S} = \sum_{i=1}^{n} V_i(S_i) = \sum_{i=1}^{n} (1/2)S_i^2, \tag{16}$$

Recalling **Lemma 1**, we can obtain the time derivative of $V(\boldsymbol{S})$ as

$$\begin{aligned} \dot{V}(\boldsymbol{S}) &= \boldsymbol{S}^T\dot{\boldsymbol{S}} = -\sum_{i=1}^{n} (\lambda_i |S_i|) \\ &= -\sqrt{2}\lambda_M \sum_{i=1}^{n} V_i^{\frac{1}{2}}(S_i) \\ &\leq -\sqrt{2}\lambda_M (\sum_{i=1}^{n} V_i(S_i))^{\frac{1}{2}} \\ &= -\sqrt{2}\lambda_M V^{\frac{1}{2}}(\boldsymbol{S}), \end{aligned} \tag{17}$$

where $\lambda_M = \min(\lambda_i)$. If $\lambda_i > 0$, it is concluded according to (17) that in finite time, states of the system will arrive at sliding hyperplane $\boldsymbol{S} = \boldsymbol{0}$. Then, we obtain the sliding motion formulated by

$$\begin{aligned} \boldsymbol{S} &= \boldsymbol{\Lambda}_r^{(4)} - (\boldsymbol{\alpha}\boldsymbol{\tau} + \boldsymbol{\xi}_0) - (\hat{\boldsymbol{\xi}}_0 - \boldsymbol{\xi}_0) + \sum_{i=1}^{3} \boldsymbol{H}_i(\boldsymbol{\Lambda}_r^{(i)} - \boldsymbol{\Lambda}_i) \\ &\quad - \sum_{i=1}^{3} \boldsymbol{H}_i(\hat{\boldsymbol{\Lambda}}_i - \boldsymbol{\Lambda}_i) + \boldsymbol{H}_0(\boldsymbol{\Lambda}_r - \boldsymbol{\Lambda}_0) \\ &= \boldsymbol{0}. \end{aligned} \tag{18}$$

Letting $\boldsymbol{E}_0 = \boldsymbol{\Lambda}_r - \boldsymbol{\Lambda}_0$, $\boldsymbol{E}_i = \boldsymbol{\Lambda}_r^{(i)} - \boldsymbol{\Lambda}_i, (i = 1, 2, 3)$, yields,

$$\begin{aligned} &\boldsymbol{\Lambda}_r^{(4)} - (\boldsymbol{\alpha}\boldsymbol{\tau} + \boldsymbol{\xi}_0) + \boldsymbol{H}_3\boldsymbol{E}_3 + \boldsymbol{H}_2\boldsymbol{E}_2 + \boldsymbol{H}_1\boldsymbol{E}_1 + \boldsymbol{H}_0\boldsymbol{E}_0 \\ &= \sum_{i=1}^{3} \boldsymbol{H}_i\boldsymbol{E}_{\Lambda_i} + \boldsymbol{E}_{\xi_0}. \end{aligned} \tag{19}$$

Combining (19) with system dynamics (5) yields

$$\begin{aligned} &\boldsymbol{E}_0^{(4)} + \boldsymbol{H}_3\boldsymbol{E}_0^{(3)} + \boldsymbol{H}_2\ddot{\boldsymbol{E}}_0 + \boldsymbol{H}_1\dot{\boldsymbol{E}}_0 + \boldsymbol{H}_0\boldsymbol{E}_0 \\ &= \sum_{i=1}^{3} \boldsymbol{H}_i\boldsymbol{E}_{\Lambda_i} + \boldsymbol{E}_{\xi_0}. \end{aligned} \tag{20}$$

Under the given conditions, it can be certified that system A is stable. Under the given conditions that $H_{i1}, H_{i2}, \cdots, H_{in} > 0$, it can be certified that system

$$\boldsymbol{E}_0^{(4)} + \boldsymbol{H}_3\boldsymbol{E}_0^{(3)} + \boldsymbol{H}_2\ddot{\boldsymbol{E}}_0 + \boldsymbol{H}_1\dot{\boldsymbol{E}}_0 + \boldsymbol{H}_0\boldsymbol{E}_0 = \boldsymbol{0}, \tag{21}$$

achieves exponential stability. One step further, it is deduced according to Lemma 5.5 in [49] that system (20) features ISS. Based on the results of observer estimation dynamics (7), $\lim_{t\to\infty} \boldsymbol{E}_{\Lambda_i}(t) = \boldsymbol{0}$, $\lim_{t\to\infty} \boldsymbol{E}_{\xi_j}(t) = \boldsymbol{0}$. Hence, it can be concluded based on **Lemma 2** that the state of system (20) satisfies $\lim_{t\to\infty} \boldsymbol{E}_0(t) = \lim_{t\to\infty}(\boldsymbol{q}_r(t) - \boldsymbol{q}_l(t)) = \boldsymbol{0}$. This suggests that link position $\boldsymbol{q}_l$ will converge to the reference trajectory $\boldsymbol{q}_r$ in an asymptotic manner under the presented control approach. The proof is thus ended.

Remark 2: Compared with the traditional SMC method, the presented approach is continuous and can effectively attenuate the chattering phenomenon attributable to the presence of the high-frequency switching item. Different from the existing CSMC [47], the proposed control method has two obvious advantages: 1) The improved dynamic sliding surface simplifies the computational burden caused by the existence of a derivative term in the original sliding surface; 2) The introduction of time-varying disturbance estimation actively enhances the disturbance suppression ability of the system; 3) It can be known from the above proof process that the recommended method only needs control gain $\lambda_i > 0$, rather than requiring λ_i to be greater than the upper limit of the time derivative of the perturbation [47]. Therefore, owing to the intrinsic structural merits, the recommended control strategy features the FJR systems with high-accuracy tracking and strong disturbance rejection capacity.

Remark 3: The coefficients of the recommended control approach can be easily configured. The method consists of two sets of control coefficients $\boldsymbol{H}_i$ and $\boldsymbol{L}_i$ ($\boldsymbol{H}_i$ in controller (13) and $\boldsymbol{L}_i$ in observer (6)), and a control gain $\boldsymbol{\lambda}$. According to the given parameter configuration rules, $\boldsymbol{H}_i$ and $\boldsymbol{L}_i$ can be determined separately, which can also be illustrated by the following simulation examples. For $\boldsymbol{\lambda}$, it satisfies $\lambda_i > 0$.

4. Simulation results

In order to substantiate the merits of the presented control approach, a comparative test between our presented control method and the well-known ADRC scheme is performed on a two-link FJR employing MATLAB/Simulink with a fixed-step solver, and its sampling period is set as 0.1ms. The ADRC method is designed as [50]

$$\boldsymbol{\tau} = \boldsymbol{\alpha}^{-1}(\boldsymbol{\Lambda}_r^{(4)} + \sum_{i=1}^{3} \boldsymbol{H}_i(\boldsymbol{\Lambda}_r^{(i)} - \hat{\boldsymbol{\Lambda}}_i) + \boldsymbol{H}_0(\boldsymbol{\Lambda}_r - \boldsymbol{\Lambda}_0) - \hat{\boldsymbol{\xi}}_0), \tag{22}$$

and the corresponding observer called ESO is formulated as

$$\begin{cases} \dot{\hat{\boldsymbol{\Lambda}}}_i = \hat{\boldsymbol{\Lambda}}_{i+1} - \boldsymbol{L}_{4-i}(\hat{\boldsymbol{\Lambda}}_0 - \boldsymbol{\Lambda}_0), \ i =, 0, 1, 2, \\ \dot{\hat{\boldsymbol{\Lambda}}}_3 = \hat{\boldsymbol{\xi}}_0 + \boldsymbol{\alpha}\boldsymbol{\tau} - \boldsymbol{L}_1(\hat{\boldsymbol{\Lambda}}_0 - \boldsymbol{\Lambda}_0), \\ \dot{\hat{\boldsymbol{\xi}}}_0 = -\boldsymbol{L}_0(\hat{\boldsymbol{\Lambda}}_0 - \boldsymbol{\Lambda}_0). \end{cases} \tag{23}$$

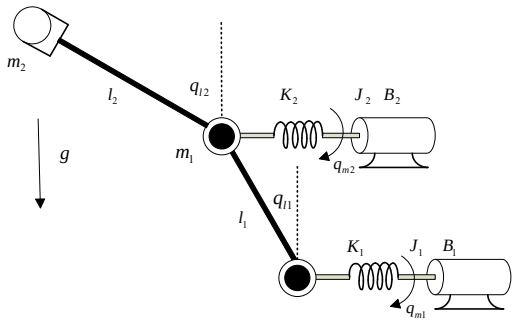

Figure 2: Two-link FJ manipulator

Fig. 2 depicts the two-link FJ manipulator. The parameters for the dynamics in the form of (1) are listed as

$$\boldsymbol{M}(\boldsymbol{q}_l) = \begin{bmatrix} (m_1 + m_2)l_1^2 & m_1 l_1 l_2(s_1 s_2 + h_1 h_2) \\ m_1 l_1 l_2(s_1 s_2 + h_1 h_2) & m_2 l_2^2 \end{bmatrix},$$

$$\boldsymbol{C}(\boldsymbol{q}_l, \dot{\boldsymbol{q}}_l) = m_2 l_1 l_2(h_1 s_2 - s_1 h_2) \begin{bmatrix} 0 & -\dot{q}_{l2} \\ -\dot{q}_{l1} & 0 \end{bmatrix},$$

$$\boldsymbol{G}(\boldsymbol{q}_l) = \begin{bmatrix} -(m_1 + m_2)l_1^2 \\ -m_2 l_2 g s_2 \end{bmatrix}, \boldsymbol{J} = \begin{bmatrix} J_1 & 0 \\ 0 & J_2 \end{bmatrix}, \boldsymbol{B} = \begin{bmatrix} B_1 & 0 \\ 0 & B_2 \end{bmatrix}, \boldsymbol{K} = \begin{bmatrix} K_1 & 0 \\ 0 & K_2 \end{bmatrix}, \boldsymbol{\tau} = \begin{bmatrix} \tau_1 \\ \tau_2 \end{bmatrix},$$

where $h_1 = \cos(q_{l1})$, $s_1 = \sin(q_{l1})$, $h_2 = \cos(q_{l2})$, $s_2 = \sin(q_{l2})$. Table 1 gives the nominal parameter values of the two-link FJR employed in the tests.

Suppose that the FJR system is perturbed by external disturbances and parameter variations. Uncertainties of $\boldsymbol{K}$, $\boldsymbol{J}$, and $\boldsymbol{M}(\boldsymbol{q}_l)$ are $\Delta K_1 = \Delta K_2 = 5\cos(0.5t)$ N·m/rad, $\Delta J_1 = \Delta J_2 = 0.2\sin(0.2t)$ kg·m^2, and $\Delta m_1 = \Delta m_2 = 0.2\sin(0.5t)$ kg, respectively. The external disturbances $\boldsymbol{d}_1$, $\boldsymbol{d}_2$ are set separately as

$$\boldsymbol{d}_1 = \begin{bmatrix} d_{11} \\ d_{12} \end{bmatrix} = \begin{cases} [2; 2], & 10 \le t < 20, \\ [2d; 2d], & 20 \le t < 30, \\ \boldsymbol{0}, & else, \end{cases} \quad \boldsymbol{d}_2 = \begin{bmatrix} d_{21} \\ d_{22} \end{bmatrix} = \begin{cases} [7; 7], & 30 \le t < 40, \\ [7d; 7d], & 40 \le t < 50, \\ \boldsymbol{0}, & else, \end{cases}$$

where $d = e^{-\sin^2(10t)}\cos^2(5t)$ (This formula refers to the expression of disturbances in literature [7] and [40]).

Table 1: Nominal parameters of two-link FJR

Parameter	Description	Values	Unit
m_1	mass of link 1	2	kg
m_2	mass of link 2	3	kg
l_1	length of link 1	1	m
l_2	length of link 2	1	m
J_1	joint flexibility	1	kg·m^2
J_2	joint flexibility	1	kg·m^2
B_1	damping coefficient	0.9	N·m·s/rad
B_2	damping coefficient	0.9	N·m·s/rad
K_1	joint stiffness	100	N·m/rad
K_2	joint stiffness	100	N·m/rad
g	gravitational constant	9.8	m/s^2

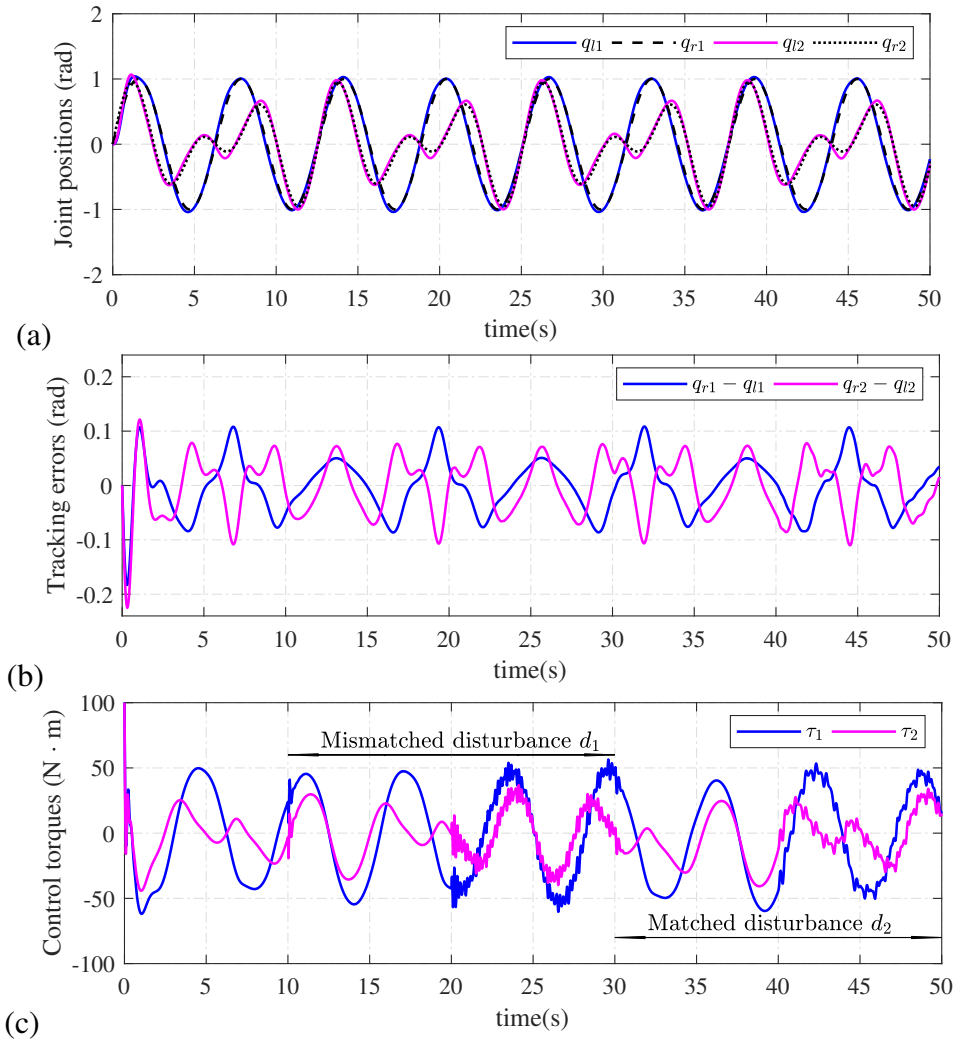

Figure 3: Response curves of two-link FJR under the ADRC approach: (a) Desired trajectories, q_{r1}, q_{r2}, and link positions, q_{l1}, q_{l2}; (b) Tracking errors, $q_{r1} - q_{l1}, q_{r2} - q_{l2}$; (c) Control torques, τ_1, τ_2.

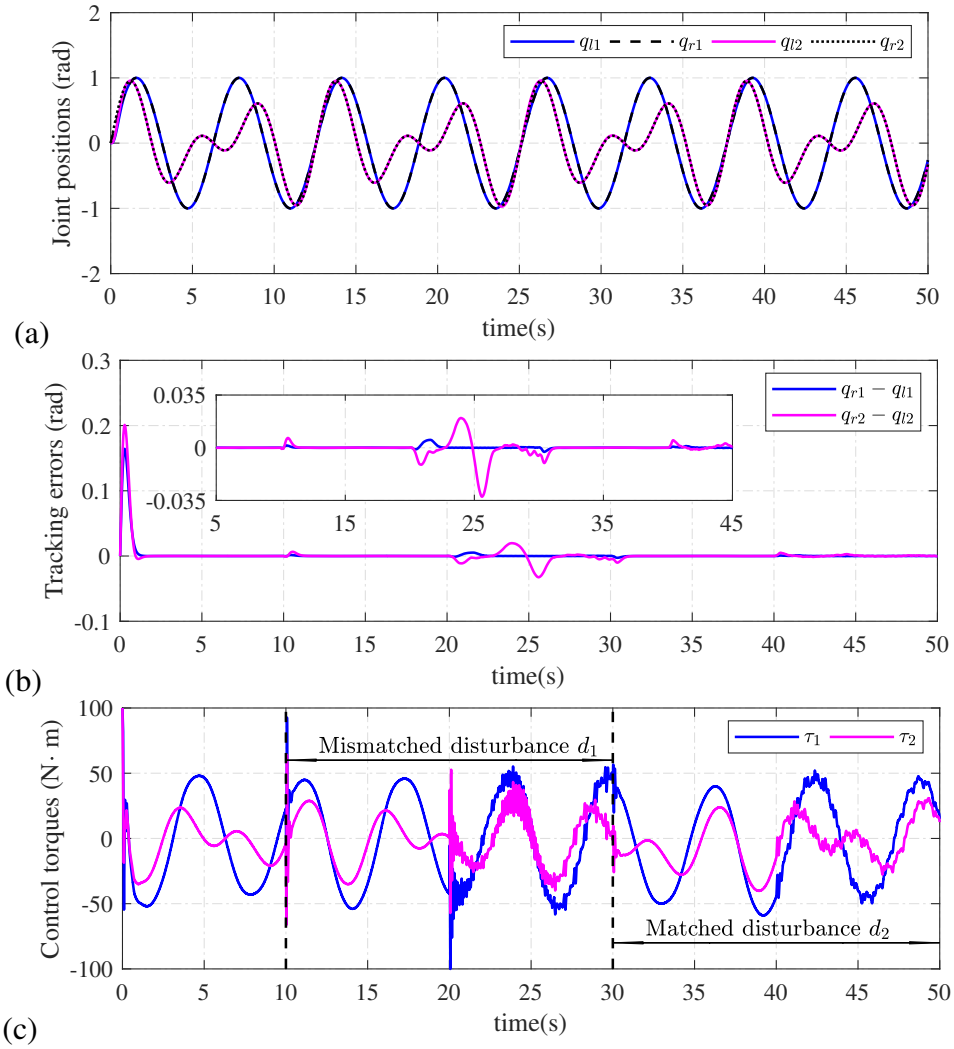

Figure 4: Response curves of two-link FJR under the presented control approach: (a) Desired trajectories, q_{r1}, q_{r2}, and link positions, q_{l1}, q_{l2}; (b) Tracking errors, $q_{r1} - q_{l1}, q_{r2} - q_{l2}$; (c) Control torques, τ_1, τ_2.

Table 2: Trajectory tracking performance comparisons

Control approach	Time period	$IAE_{q_{l1}}$	$IAE_{q_{l2}}$	$ITAE_{q_{l1}}$	$ITAE_{q_{l2}}$
ADRC	0-10 seconds	0.4808	0.5389	2.2037	2.1948
	10-30 seconds	0.7354	0.8552	7.7594	8.6446
	30-50 seconds	0.7428	0.8588	7.3013	8.5130
Proposed scheme	0-10 seconds	0.0839	0.1003	0.0335	0.0390
	10-30 seconds	0.0075	0.0754	0.0789	1.0548
	30-50 seconds	0.0032	0.0146	0.0212	0.1145

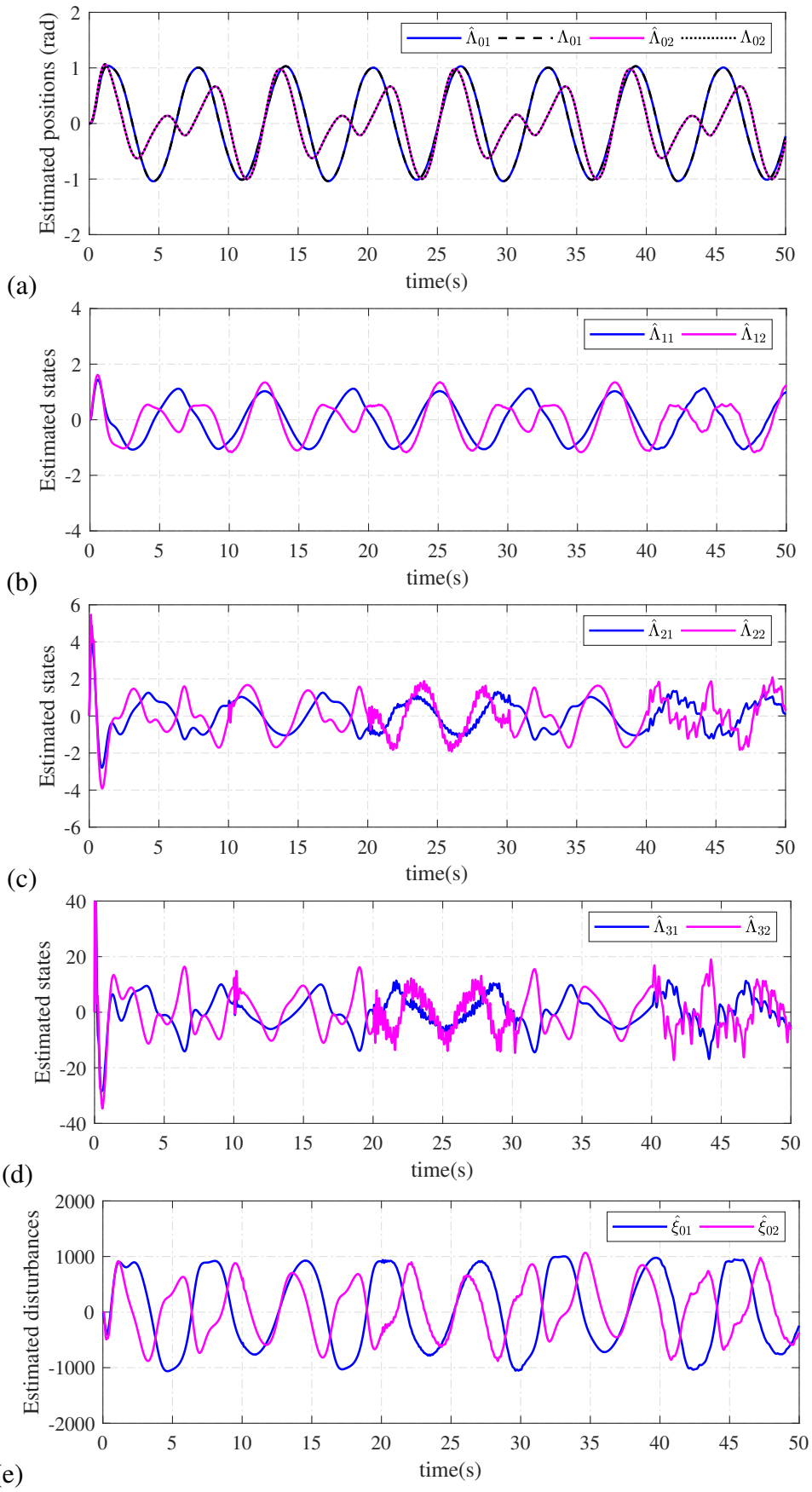

Figure 5: Estimate curves of two-link FJR under the ADRC approach: (a) Link positions, $\Lambda_{01}, \Lambda_{02}$, and its estimates, $\hat{\Lambda}_{01}, \hat{\Lambda}_{02}$; (b) Estimated states, $\hat{\Lambda}_{11}, \hat{\Lambda}_{12}$; (c) Estimated states, $\hat{\Lambda}_{21}, \hat{\Lambda}_{22}$; (d) Estimated states, $\hat{\Lambda}_{31}, \hat{\Lambda}_{32}$; (e) Estimated disturbances, $\hat{\xi}_{01}, \hat{\xi}_{02}$.

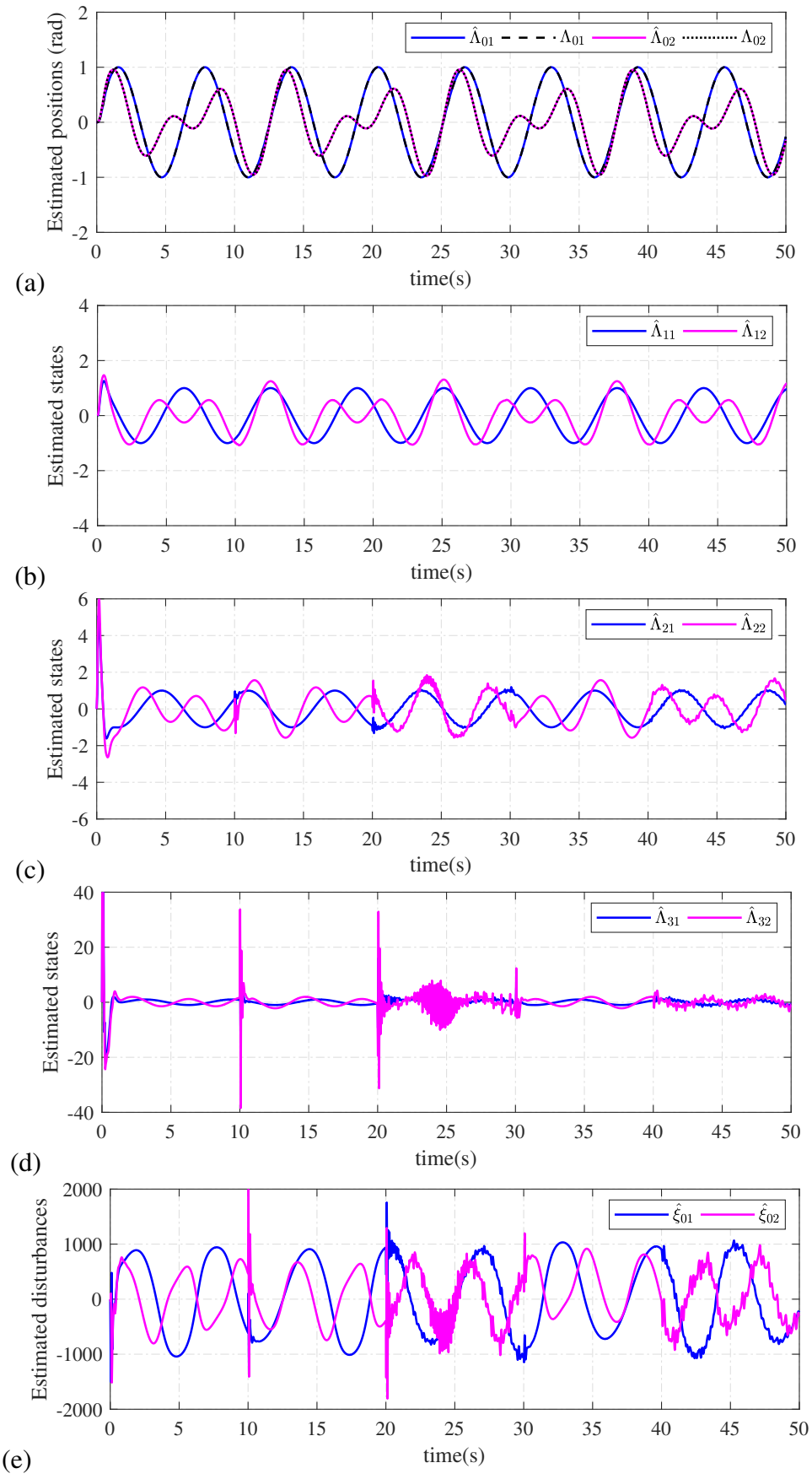

Figure 6: Estimate curves of two-link FJR under the presented control approach: (a) Link positions, $\Lambda_{01}, \Lambda_{02}$, and its estimates, $\hat{\Lambda}_{01}, \hat{\Lambda}_{02}$; (b) Estimated states, $\hat{\Lambda}_{11}, \hat{\Lambda}_{12}$; (c) Estimated states, $\hat{\Lambda}_{21}, \hat{\Lambda}_{22}$; (d) Estimated states, $\hat{\Lambda}_{31}, \hat{\Lambda}_{32}$; (e) Estimated disturbances, $\hat{\xi}_{01}, \hat{\xi}_{02}$.

Let the desired trajectories be

$$q_{r1} = \sin(t),$$
$$q_{r2} = 0.5\sin(t) + 0.5\sin(1.5t).$$

Choosing m in (6) as $m = 5$, the observer coefficients and controller gains of the proposed control method in (6) and (13) are designed as

$$\begin{aligned}
&\boldsymbol{L}_0 = \mathrm{diag}(\omega_o^9, \omega_o^9), && \boldsymbol{L}_1 = \mathrm{diag}(9\omega_o^8, 9\omega_o^8),\\
&\boldsymbol{L}_2 = \mathrm{diag}(36\omega_o^7, 36\omega_o^7), && \boldsymbol{L}_3 = \mathrm{diag}(84\omega_o^6, 84\omega_o^6),\\
&\boldsymbol{L}_4 = \mathrm{diag}(126\omega_o^5, 126\omega_o^5), && \boldsymbol{L}_5 = \mathrm{diag}(126\omega_o^4, 126\omega_o^4),\\
&\boldsymbol{L}_6 = \mathrm{diag}(84\omega_o^3, 84\omega_o^3), && \boldsymbol{L}_7 = \mathrm{diag}(36\omega_o^2, 36\omega_o^2),\\
&\boldsymbol{L}_8 = \mathrm{diag}(9\omega_o, 9\omega_o), && \boldsymbol{\lambda} = \mathrm{diag}(2500, 2500),\\
&\boldsymbol{H}_0 = \mathrm{diag}(\omega_c^4, \omega_c^4), && \boldsymbol{H}_1 = \mathrm{diag}(4\omega_c^3, 4\omega_c^3),\\
&\boldsymbol{H}_2 = \mathrm{diag}(6\omega_c^2, 6\omega_c^2), && \boldsymbol{H}_3 = \mathrm{diag}(4\omega_c, 4\omega_c),
\end{aligned}$$

where $\omega_c = 9$, $\omega_o = 40$. In the interest of an equitable comparison, coefficients of the ADRC scheme are set to: $\boldsymbol{H}_i$ in (22) is identical to that in (13), the observer bandwidth of ESO is also set as $\omega_o = 40$, and thus $\boldsymbol{L}_i$ in (23) is configured as

$$\begin{aligned}
&\boldsymbol{L}_0 = \mathrm{diag}(\omega_o^5, \omega_o^5), && \boldsymbol{L}_1 = \mathrm{diag}(5\omega_o^4, 5\omega_o^4),\\
&\boldsymbol{L}_2 = \mathrm{diag}(10\omega_o^3, 10\omega_o^3), && \boldsymbol{L}_3 = \mathrm{diag}(10\omega_o^2, 10\omega_o^2),\\
&\boldsymbol{L}_4 = \mathrm{diag}(5\omega_o, 5\omega_o).
\end{aligned}$$

The saturated limits of control input $\boldsymbol{\tau}$ is set to $\tau_i \in [-100, +100]$ for both methods.

There are three groups of tests that we performed to evaluate the robustness and tracking performance of the two-link FJR system under ADRC and proposed robust control schemes. The test results of these two approaches are displayed in Figs.3-6, respectively, where $\hat{\Lambda}_{i1}$ and $\hat{\Lambda}_{i2}$ are the components of $\hat{\Lambda}_i$, $(i = 0, 1, 2, 3)$, respectively, and $\hat{\xi}_{01}$ and $\hat{\xi}_{02}$ are the components of $\hat{\xi}_0$.

Response profiles of desired trajectories q_{r1}, q_{r2}, real-time trajectories q_{l1}, q_{l2}, tracking errors $q_{r1} - q_{l1}, q_{r2} - q_{l2}$, and control torques τ_1, τ_2 of link 1 and link 2 of the two-link FJR, are shown in Fig. 3 and Fig. 4. Corresponding to Fig. 3 and Fig. 4, estimate curves of link position estimates $\hat{\Lambda}_{01}, \hat{\Lambda}_{02}$, estimated states $\hat{\Lambda}_{11}, \hat{\Lambda}_{12}$, $\hat{\Lambda}_{21}, \hat{\Lambda}_{22}$, $\hat{\Lambda}_{31}, \hat{\Lambda}_{32}$, and estimated disturbances $\hat{\xi}_{01}, \hat{\xi}_{02}$ are respectively provided in Fig. 5 and Fig. 6.

The first comparative tests are shown in Figs.3-6 for 0-10 seconds, where parameter uncertainties Δm_i, ΔJ_i, ΔK_i are considered. As observed in Fig. 3(b) and Fig. 4(b), when the ADRC and recommended continuous output feedback control methods are respectively employed to the two-link FJR, the system under the ADRC scheme possesses larger tracking errors compared with the proposed control method. These curves indicate that the presented control method has higher precision tracking performance and can suppress parameter uncertainties. During 10-20 seconds, the second comparative test is conducted to verify the robustness against mismatched disturbance $\boldsymbol{d}_1$, which perturbs the link of the two-link FJR. It is displayed from Fig. 4(b) that the presented control method obtains a stronger ability to suppress mismatched disturbance. The third comparative test is conducted in 20-30 seconds to examine the capacity of the system to handle matched disturbance $\boldsymbol{d}_2$. From the results of Fig. 3(b) and Fig. 4(b), we can observe that the proposed output feedback controller possesses a smaller tracking error, which indicates that the system under the proposed approach has the ability to suppress matched disturbance. To quantify the tracking performance of the system, integral absolute

error (IAE) and integral time-weighted absolute error (ITAE) are introduced, which are defined as $IAE_{q_{li}} = \int_{t_0}^{t} |q_{ri} - q_{li}| d\tau, (i = 1, 2)$, $ITAE_{q_{lj}} = \int_{t_0}^{t} (\tau - t_0)|q_{rj} - q_{lj}| d\tau, (j = 1, 2)$. According to Figs 3-4, the comparison of performance indexes on the ADRC and proposed strategies at diverse conditions are revealed in Table 2. It can be concluded that the presented control strategy achieves excellent high-precision tracking performance and strong disturbance rejection capacity.

5. Conclusions

This paper has addressed the tracking control issue of generic underactuated FJR systems bearing the brunt of unknown unmatched/matched time-varying disturbances, covering parameter uncertainties, changing operating circumstances, etc. To eliminate the adverse effects of these disturbances on control performance, a GPIO is firstly devised based on a simplified model where the mismatched disturbances are transferred to the matched ones by the means of the flatness technique. Then, an output feedback control framework using the CSMC technique is developed with the aid of the estimated perturbation and states provided by the GPIO. The proposed control approach ensures that system output asymptotically converges its desired trajectory and keeps a continuous control behavior. Besides, only the position measurements of the link side are employed for the design of the developed GPIO and control law. Moreover, the comparative results on the two-link FJR have shown that overall the proposed robust control method outperforms the conventional ADRC scheme in the existence of various matched/unmatched perturbations. Due to the complete theoretic guarantee and the simple control structure of the presented control approach, it can be easily extended to other similar disturbed systems with mild modification.

Acknowledgements

This work was supported in part the Natural Science Foundation Project of Chongqing, China (cstc2021jcyj-msxmX0142), in part by the Cooperative Project between Universities in Chongqing and Affiliated Institutes of Chinese Academy of Sciences, China (HZ2021018), and in part by the Innovation Research Group of Universities in Chongqing, China (CXQT20016).

Appendix

The expression of $\boldsymbol{\tau}$ in (3) is governed by

$$
\begin{aligned}
\boldsymbol{\tau} &= \boldsymbol{J}\dot{\boldsymbol{x}}_4 + \boldsymbol{B}\boldsymbol{x}_4 + \boldsymbol{K}(\boldsymbol{x}_3 - \boldsymbol{x}_1) - \boldsymbol{d}_2 \\
&= \frac{\boldsymbol{J}}{\boldsymbol{K}}\Big(\boldsymbol{M}(\boldsymbol{\Lambda})\boldsymbol{\Lambda}^{(4)} + 2\dot{\boldsymbol{M}}(\boldsymbol{\Lambda})\boldsymbol{\Lambda}^{(3)} + \ddot{\boldsymbol{M}}(\boldsymbol{\Lambda})\ddot{\boldsymbol{\Lambda}} \\
&\quad + \boldsymbol{C}(\boldsymbol{\Lambda},\dot{\boldsymbol{\Lambda}})\boldsymbol{\Lambda}^{(3)} + 2\dot{\boldsymbol{C}}(\boldsymbol{\Lambda},\dot{\boldsymbol{\Lambda}})\ddot{\boldsymbol{\Lambda}} + \ddot{\boldsymbol{C}}(\boldsymbol{\Lambda},\dot{\boldsymbol{\Lambda}})\dot{\boldsymbol{\Lambda}} + \boldsymbol{K}\ddot{\boldsymbol{\Lambda}} \\
&\quad + \ddot{\boldsymbol{G}}(\boldsymbol{\Lambda}) - \ddot{\boldsymbol{d}}_1\Big) + \frac{\boldsymbol{B}}{\boldsymbol{K}}\Big(\boldsymbol{M}(\boldsymbol{\Lambda})\boldsymbol{\Lambda}^{(3)} + \dot{\boldsymbol{M}}(\boldsymbol{\Lambda})\ddot{\boldsymbol{\Lambda}} \\
&\quad + \boldsymbol{C}(\boldsymbol{\Lambda},\dot{\boldsymbol{\Lambda}})\ddot{\boldsymbol{\Lambda}} + \dot{\boldsymbol{C}}(\boldsymbol{\Lambda},\dot{\boldsymbol{\Lambda}})\dot{\boldsymbol{\Lambda}} + \boldsymbol{K}\dot{\boldsymbol{\Lambda}} + \dot{\boldsymbol{G}}(\boldsymbol{\Lambda}) - \dot{\boldsymbol{d}}_1\Big) \\
&\quad + \boldsymbol{M}(\boldsymbol{\Lambda})\ddot{\boldsymbol{\Lambda}} + \boldsymbol{C}(\boldsymbol{\Lambda},\dot{\boldsymbol{\Lambda}})\dot{\boldsymbol{\Lambda}} + \boldsymbol{G}(\boldsymbol{\Lambda}) - \boldsymbol{d}_1 - \boldsymbol{d}_2 \\
&= \frac{\boldsymbol{J}\boldsymbol{M}(\boldsymbol{\Lambda})}{\boldsymbol{K}}\boldsymbol{\Lambda}^{(4)} + \frac{2\boldsymbol{J}\dot{\boldsymbol{M}}(\boldsymbol{\Lambda}) + \boldsymbol{B}\boldsymbol{M}(\boldsymbol{\Lambda}) + \boldsymbol{J}\boldsymbol{C}(\boldsymbol{\Lambda},\dot{\boldsymbol{\Lambda}})}{\boldsymbol{K}}\boldsymbol{\Lambda}^{(3)} \\
&\quad + \Big(\frac{\boldsymbol{J}\ddot{\boldsymbol{M}}(\boldsymbol{\Lambda}) + 2\boldsymbol{J}\dot{\boldsymbol{C}}(\boldsymbol{\Lambda},\dot{\boldsymbol{\Lambda}})}{\boldsymbol{K}} + \frac{\boldsymbol{B}\dot{\boldsymbol{M}}(\boldsymbol{\Lambda}) + \boldsymbol{B}\boldsymbol{C}(\boldsymbol{\Lambda},\dot{\boldsymbol{\Lambda}})}{\boldsymbol{K}} \\
&\quad + \boldsymbol{M}(\boldsymbol{\Lambda}) + \boldsymbol{J}\Big)\ddot{\boldsymbol{\Lambda}} + \Big(\frac{\boldsymbol{J}\ddot{\boldsymbol{C}}(\boldsymbol{\Lambda},\dot{\boldsymbol{\Lambda}})}{\boldsymbol{K}} + \frac{\boldsymbol{B}\dot{\boldsymbol{C}}(\boldsymbol{\Lambda},\dot{\boldsymbol{\Lambda}})}{\boldsymbol{K}} \\
&\quad + \boldsymbol{C}(\boldsymbol{\Lambda},\dot{\boldsymbol{\Lambda}}) + \boldsymbol{B}\Big)\dot{\boldsymbol{\Lambda}} + \frac{\boldsymbol{J}}{\boldsymbol{K}}\Big(\ddot{\boldsymbol{G}}(\boldsymbol{\Lambda}) - \ddot{\boldsymbol{d}}_1\Big) \\
&\quad + \frac{\boldsymbol{B}}{\boldsymbol{K}}\Big(\dot{\boldsymbol{G}}(\boldsymbol{\Lambda}) - \dot{\boldsymbol{d}}_1\Big) + \boldsymbol{G}(\boldsymbol{\Lambda}) - \boldsymbol{d}_1 - \boldsymbol{d}_2.
\end{aligned}
$$

References

[1] Y. Pan, H. Wang, X. Li, H. Yu, Adaptive command-filtered backstepping control of robot arms with compliant actuators, IEEE Transactions on Control Systems Technology 26 (3) (2017) 1149–1156.

[2] X. Li, Y. Pan, G. Chen, H. Yu, Multi-modal control scheme for rehabilitation robotic exoskeletons, The International Journal of Robotics Research 36 (5-7) (2017) 759–777.

[3] J. Moreno-Valenzuela, C. Aguilar-Avelar, Motion control of underactuated mechanical systems, Vol. 1, Springer, 2018.

[4] H. Wang, Y. Zhang, Z. Zhao, X. Tang, J. Yang, I.-M. Chen, Finite-time disturbance observer-based trajectory tracking control for flexible-joint robots, Nonlinear Dynamics 106 (1) (2021) 459–471.

[5] M. W. Spong, Underactuated mechanical systems, in: Control Problems in Robotics and Automation, Springer, 1998, pp. 135–150.

[6] Y.-C. Chang, H.-M. Yen, Robust tracking control for a class of electrically driven flexible-joint robots without velocity measurements, International Journal of Control 85 (2) (2012) 194–212.

[7] H. Wang, Y. Pan, S. Li, H. Yu, Robust sliding mode control for robots driven by compliant actuators, IEEE Transactions on Control Systems Technology 27 (3) (2018) 1259–1266.

[8] S. Ling, H. Wang, P. X. Liu, Adaptive fuzzy tracking control of flexible-joint robots based on command filtering, IEEE Transactions on Industrial Electronics 67 (5) (2019) 4046–4055.

[9] X. Li, Y. Pan, G. Chen, H. Yu, Adaptive human-robot interaction control for robots driven by series elastic actuators, IEEE Transactions on Robotics 33 (1) (2016) 169–182.

[10] W. Sun, S.-F. Su, J. Xia, V.-T. Nguyen, Adaptive fuzzy tracking control of flexible-joint robots with full-state constraints, IEEE transactions on Systems, Man, and Cybernetics: Systems 49 (11) (2018) 2201–2209.

[11] H. Gao, W. He, C. Zhou, C. Sun, Neural network control of a two-link flexible robotic manipulator using assumed mode method, IEEE Transactions on Industrial Informatics 15 (2) (2018) 755–765.

[12] Y. Pan, X. Li, H. Wang, H. Yu, Continuous sliding mode control of compliant robot arms: A singularly perturbed approach, Mechatronics 52 (2018) 127–134.

[13] Y. Pan, X. Li, H. Yu, Efficient pid tracking control of robotic manipulators driven by compliant actuators, IEEE Transactions on Control Systems Technology 27 (2) (2019) 915–922.

[14] Q. Zhang, G. Liu, Precise control of elastic joint robot using an interconnection and damping assignment passivity-based approach, IEEE/ASME Transactions on Mechatronics 21 (6) (2016) 2728–2736.
[15] M. Ruderman, M. Iwasaki, W.-H. Chen, Motion-control techniques of today and tomorrow: A review and discussion of the challenges of controlled motion, IEEE Industrial Electronics Magazine 14 (1) (2020) 41–55.
[16] S. Li, J. Yang, W.-H. Chen, X. Chen, Disturbance observer-based control: methods and applications, CRC Press, 2014.
[17] X. Wang, S. Li, X. Yu, J. Yang, Distributed active anti-disturbance consensus for leader-follower higher-order multi-agent systems with mismatched disturbances, IEEE Transactions on Automatic Control 62 (11) (2016) 5795–5801.
[18] Y. Yan, J. Yang, C. Liu, M. Coombes, S. Li, W.-H. Chen, On the actuator dynamics of dynamic control allocation for a small fixed-wing uav with direct lift control, IEEE Transactions on Control Systems Technology 28 (3) (2020) 984–991.
[19] S. Ding, J. H. Park, C.-C. Chen, Second-order sliding mode controller design with output constraint, Automatica 112 (2020) 108704.
[20] J. Yang, S. Li, X. Yu, Sliding-mode control for systems with mismatched uncertainties via a disturbance observer, IEEE Transactions on Industrial Electronics 60 (1) (2012) 160–169.
[21] Y. Shtessel, C. Edwards, L. Fridman, A. Levant, Sliding mode control and observation, Springer, 2014.
[22] Z. Zhao, J. Yang, S. Li, Z. Zhang, L. Guo, Finite-time super-twisting sliding mode control for mars entry trajectory tracking, Journal of the Franklin Institute 352 (11) (2015) 5226–5248.
[23] X. Wang, G. Wang, S. Li, K. Lu, Composite sliding-mode consensus algorithms for higher-order multi-agent systems subject to disturbances, IET Control Theory & Applications 14 (2) (2020) 291–303.
[24] M. R. Soltanpour, M. Moattari, et al., Voltage based sliding mode control of flexible joint robot manipulators in presence of uncertainties, Robotics and Autonomous Systems 118 (2019) 204–219.
[25] P. V. Suryawanshi, P. D. Shendge, S. B. Phadke, A boundary layer sliding mode control design for chatter reduction using uncertainty and disturbance estimator, International Journal of Dynamics and Control 4 (4) (2016) 456–465.
[26] L. Zouari, H. Abid, M. Abid, Sliding mode and PI controllers for uncertain flexible joint manipulator, International Journal of Automation and Computing 12 (2) (2015) 117–124.
[27] K. Rsetam, Z. Cao, Z. Man, M. Mitrevska, Optimal second order integral sliding mode control for a flexible joint robot manipulator, in: IECON 2017-43rd Annual Conference of the IEEE Industrial Electronics Society, IEEE, 2017, pp. 3069–3074.
[28] A. Filipescu, L. Dugard, J.-M. Dion, Adaptive gain sliding observer based sliding controller for uncertain parameters nonlinear systems. application to flexible joint robots, in: 42nd IEEE International Conference on Decision and Control (IEEE Cat. No. 03CH37475), Vol. 4, IEEE, 2003, pp. 3537–3542.
[29] S. Ding, S. Li, Second-order sliding mode controller design subject to mismatched term, Automatica 77 (2017) 388–392.
[30] J. Yang, Z. Ding, S. Li, C. Zhang, Continuous finite-time output regulation of nonlinear systems with unmatched time-varying disturbances, IEEE Control Systems Letters 2 (1) (2017) 97–102.
[31] H. Du, G. Wen, Y. Cheng, W. Lu, T. Huang, Designing discrete-time sliding mode controller with mismatched disturbances compensation, IEEE Transactions on Industrial Informatics 16 (6) (2019) 4109–4118.
[32] A.-C. Huang, Y.-C. Chen, Adaptive sliding control for single-link flexible-joint robot with mismatched uncertainties, IEEE Transactions on Control Systems Technology 12 (5) (2004) 770–775.
[33] K. A. Rsetam, Z. Cao, Z. Man, Cascaded extended state observer based sliding mode control for underactuated flexible joint robot, IEEE Transactions on Industrial Electronics (2019).
[34] J. Huang, S. Ri, T. Fukuda, Y. Wang, A disturbance observer based sliding mode control for a class of underactuated robotic system with mismatched uncertainties, IEEE Transactions on Automatic Control 64 (6) (2018) 2480–2487.
[35] X. Li, Y.-H. Liu, H. Yu, Iterative learning impedance control for rehabilitation robots driven by series elastic actuators, Automatica 90 (2018) 1–7.
[36] S. E. Talole, J. P. Kolhe, S. B. Phadke, Extended-state-observer-based control of flexible-joint system with experimental validation, IEEE Transactions on Industrial Electronics 57 (4) (2009) 1411–1419.
[37] Y. Yan, J. Yang, Z. Sun, S. Li, H. Yu, Non-linear-disturbance-observer-enhanced MPC for motion control systems with multiple disturbances, IET Control Theory & Applications 14 (1) (2019) 63–72.
[38] B. Fu, S. Li, X. Wang, L. Guo, Output feedback based simultaneous stabilization of two port-controlled hamiltonian systems with disturbances, Journal of the Franklin Institute 356 (15) (2019) 8154–8166.
[39] Y. Yan, C. Zhang, C. Liu, J. Yang, S. Li, Disturbance rejection for nonlinear uncertain systems with output measurement errors: Application to a helicopter model, IEEE Transactions on Industrial Informatics 16 (5)

(2019) 3133–3144.
[40] H. Sira-Ramírez, J. Linares-Flores, C. García-Rodríguez, M. A. Contreras-Ordaz, On the control of the permanent magnet synchronous motor: An active disturbance rejection control approach, IEEE Transactions on Control Systems Technology 22 (5) (2014) 2056–2063.
[41] S. Zaare, M. R. Soltanpour, Continuous fuzzy nonsingular terminal sliding mode control of flexible joints robot manipulators based on nonlinear finite time observer in the presence of matched and mismatched uncertainties, Journal of the Franklin Institute (2020).
[42] J. Yang, S. Li, J. Su, X. Yu, Continuous nonsingular terminal sliding mode control for systems with mismatched disturbances, Automatica 49 (7) (2013) 2287–2291.
[43] Y.-C. Chang, H.-M. Yen, Design of a robust position feedback tracking controller for flexible-joint robots, IET Control Theory & Applications 5 (2) (2011) 351–363.
[44] M. Fliess, J. Lévine, P. Martin, P. Rouchon, Flatness and defect of non-linear systems: introductory theory and examples, International Journal of Control 61 (6) (1995) 1327–1361.
[45] J. Mao, J. Yang, S. Li, Y. Yan, Q. Li, Output feedback-based sliding mode control for disturbed motion control systems via a higher-order eso approach, IET Control Theory & Applications 12 (15) (2018) 2118–2126.
[46] Z. Wang, S. Li, J. Wang, Q. Li, Robust control for disturbed buck converters based on two GPI observers, Control Engineering Practice 66 (2017) 13–22.
[47] F. Yong, F. Han, X. Yu, Chattering free full-order sliding-mode control, Automatica 50 (4) (2014) 1310–1314.
[48] E. F. Beckenbach, R. Bellman, Inequalities, Vol. 30, Springer Science & Business Media, 2012.
[49] H. K. Khalil, Nonlinear systems, Macmilllan, London, UK (1996).
[50] J. Han, From PID to active disturbance rejection control, IEEE transactions on Industrial Electronics 56 (3) (2009) 900–906.